Constant Volume Gate-Opening by Freezing Rotational Dynamics in Microporous Organically Pillared Layered Silicates

Kilian Bärwinkel,[||] Markus M. Herling,[†] Martin Rieß,[†] Hiroshi Sato,[‡] Liangchun Li,[§] Yamini S. Avadhut,[||] Tobias W. Kemnitzer,[||] Hussein Kalo,[†] Jürgen Senker,*[,||] Ryotaro Matsuda,*[,§,⊥] Susumu Kitagawa,*[,§] and Josef Breu*[,†] [ID]

[†]Bavarian Polymer Institute and Inorganic Chemistry I, University of Bayreuth, Universitätsstraße 30, 95440 Bayreuth, Germany

[‡]Department of Chemistry and Biotechnology, School of Engineering, the University of Tokyo, 7-3-1 Hongo, Bunkyo-ku, Tokyo 113-8656, Japan

[§]Institute for Integrated Cell-Material Sciences (WPI-iCeMS), Kyoto University, Kyoto 615-8510, Japan

[||]Inorganic Chemistry III, University of Bayreuth, Universitätsstraße 30, 95440 Bayreuth, Germany

[⊥]Department of Applied Chemistry, Graduate School of Engineering, Nagoya University, School of Engineering bldg. 1, Furo-cho, Chikusa-ku, Nagoya 464-8603, Japan

S *Supporting Information*

ABSTRACT: Microporous organically pillared layered silicates (MOPS) are a class of microporous hybrid materials that, by varying pillar density, allows for optimization of guest recognition without the need to explore different framework topologies. MOPS are found to be capable of discriminating two very similar gases, carbon dioxide and acetylene, by selective gate-opening solely through quenching pillar dynamics. Contrary to conventional gate-opening in metal organic frameworks, the additional adsorption capacity is realized without macroscopic volume changes, thus avoiding mechanical stress on the framework. Of the two gases studied, only CO_2 can accomplish freezing of pillar dynamics. Moreover, the shape of the slit-type micropores in MOPS can easily

be fine-tuned by reducing the charge density of the silicate layers. This concomitantly reduces the Coulomb attraction of cationic interlayer space and anionic host layers. Surprisingly, we found that reducing the charge density then alters the gate-opening mechanism to a conventional structural gate-opening involving an increase in volume.
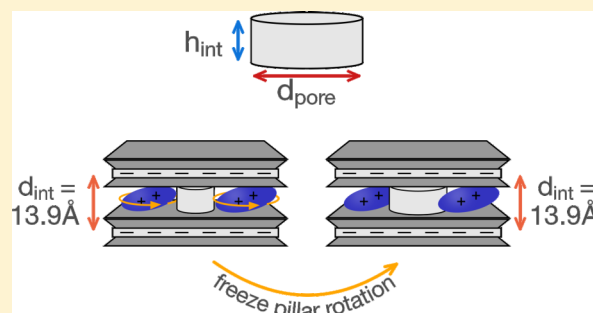
INTRODUCTION

Energy efficient gas separation is a key process in manufacturing of bulk chemicals made from gaseous starting materials.[1,2] Size-related sieving,[3−6] reversible chemical binding,[6−9] or gate-opening[10] in flexible microporous frameworks represent the corresponding main mechanisms. For the latter, the volume change associated with breathing or contraction[11] of the flexible lattice represents a serious limitation. In conventional gate-opening in metal organic frameworks (MOFs),[3,12,13] the additional adsorption capacity is realized with macroscopic volume changes, thus creating mechanical stress on the framework.

Microporous organically pillared layered silicates (MOPS) represent a largely unnoticed[1,14] class of microporous hybrid materials that are prepared by intercalation of cationic molecules, such as metal complexes or organocations, in the interlayer space of layered silicates. These molecular "pillars" may be varied in charge, size, and shape, and may be decorated with functional groups for improving selectivity. In MOPS, the pillars are held in place by nondirectional electrostatic interactions allowing for both pillar rotation and framework

flexibility, which in turn permits breathing and gate-opening similar to porous coordination polymers (PCPs) and (MOFs).

Narrow pore size distributions and a high degree of long-range order of the pillar arrays[15,16] require layered silicates with homogeneous charge densities as recently made accessible on a large scale by an expeditious melt synthesis.[17] MOPS are thermally and hydrolytically stable as the stability is only limited by that of the pillars, which is typically well above 250 °C.

The electrostatic attraction between pillars and host layers thrives to minimize the height of the interlayer space. Consequently elliptical pillars will orient with their longer principal axis in the plane of the interlayer space and the micropores of MOPS are of slit shape (Figure 1). While the width of the slits is defined by the free volume between the pillars, the height is defined by the shorter principal axis of the pillar and corresponds to the height of the interlayer space (h_{int}). The interlayer distance as determined by X-ray
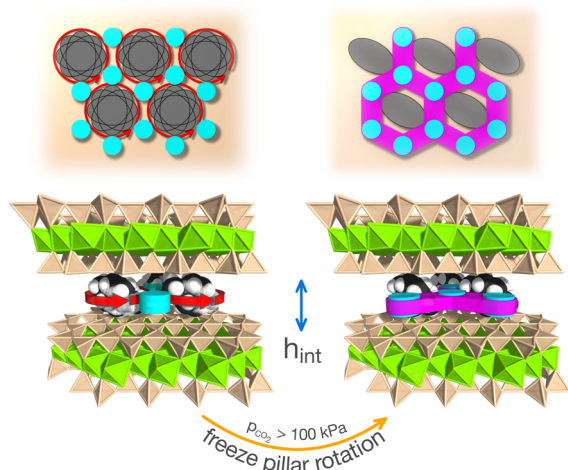
Figure 1. Constant volume gate-opening in MOPS by freezing pillar rotation. Mobil pillars (left) occupy a larger interlayer volume (gray area) that limits adsorption to the blue cylindrical micropores between three adjacent pillars. By freezing pillar rotation additionally, the pink volume becomes accessible.

diffraction measurements is the sum of h_{int} and the thickness of the silicate layer (0.97 nm).

We present herein two MOPS (MOPS-5, MOPS-6) that differ in the magnitude of the negative layer charge and therefore in density of the same organic pillar.

RESULTS AND DISCUSSION

A synthetic stevensite ($Na_{(x+2y)}[Mg_{6-(x+y)}Li_x \square_y]Si_8O_{20}F_4$) with charge densities $x = 0.44-0.49$ (MOPS-5) and $x = 0.36-0.40$ (MOPS-6) was intercalated with 1,4-dimethl-1,4-diazabicyclo [2.2.2]octane (Me$_2$DABCO^{2+}). The charge densities of the layers were determined by the so-called Lagaly method.[18] As determined by Ar physisorption analysis, both MOPS show narrow pore size distributions with d_{50}-micropore widths increasing from 4.8 Å for MOPS-5 to 5.5 Å for MOPS-6 (Figure S1 and S2). A similar trend with somewhat larger absolute values is observed based on the ^{129}Xe MAS spectra (Figure S3). For the high temperature limit, both compounds feature sharp resonances at 138.3 ppm (MOPS-5) and 122.0 ppm (MOPS-6) and a spectral width of 11 ppm corresponding to mean diameters of 6.0 Å (MOPS-5) and 6.4 Å (MOPS-6) with a distribution of roughly ±0.5 Å assuming cylindrical pore characteristic and applicability of the Fraissard model.[19,20] The downfield tail of the ^{129}Xe resonance of MOPS-6, additionally, suggests that the charge reduction induces some heterogeneity with smaller pores stretching down to 5.9 Å. The X-ray diffraction pattern of MOPS-5 and MOPS-6 both showed a rational $00l$-series with an interlayer distance of 13.9(1) Å (Figure S4) indicating a strictly uniform h_{int}. Moreover, both MOPS exhibit the same interlayer distance h_{int} as determined by the shorter principal axis of Me$_2$DABCO^{2+}, whereas the pillar separation is increased when the charge density is reduced from MOPS-5 to MOPS-6.

Despite the lack of a rigid linkage between interlayer space and silicate layers, the pillars seem to be regularly distributed resulting in two-dimensional pore networks. This two-dimensionality of the pore structure of MOPS-5 and MOPS-6 is furthermore confirmed by the anisotropic chemical shift lineshapes of the wide-line ^{129}Xe spectra (Figure S3), which change from a deshielded to a shielded characteristic with

decreasing temperature.[20] Regularity in pillar separation is driven by the repulsive forces between the cationic pillars.

Reducing the charge density as with MOPS-6 not only increases the pillar separation but concomitantly reduces the Coulomb attraction between pillars and silicate layers rendering expansion of the interlayer height more feasible. Although translational movements of pillars within the interlayer space are strongly retarded by electrostatics, pillars might show a high rotational mobility. Consequently, nonspherical pillars will occupy a dynamic volume (Figure 1) that might indeed decrease effective micropore volume accessible to adsorbents. Our concept is based on creating additional free volume for adsorption by freezing pillar rotation (Figure 1).

The adsorption isotherm of MOPS-5 for C_2H_2 exhibits a normal type I shape (Figure 2a) with a total uptake of 36
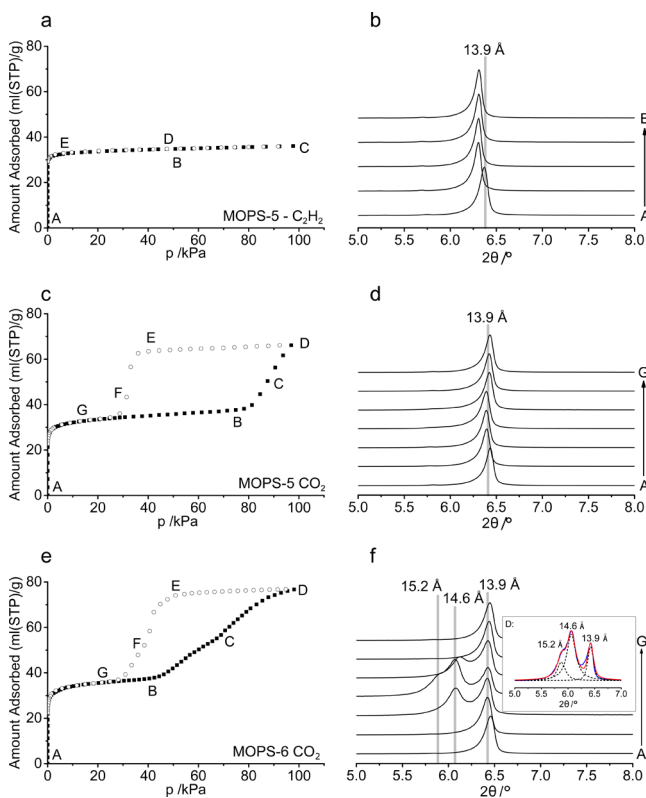
Figure 2. Adsorption isotherms measured at 195 K and in situ measured X-ray diffraction patterns in the basal reflection region for (top) C_2H_2 on MOPS-5, (middle) CO_2 on MOPS-5, and (bottom) CO_2 on MOPS-6.

cm^3(STP)/g and a constant d_{001}-value (Figure 2b) over the entire pressure range. In contrast, the corresponding adsorption isotherm for CO_2 shows a stepwise adsorption, which is unusual for common microporous materials. In the low pressure range, an initial uptake of 33.5 cm^3(STP)/g of CO_2 at 20.6 kPa is observed associated with a first plateau (Figure 2c). Beyond a threshold pressure of about 80 kPa, a gate-opening is observed, approximately doubling the total amount of adsorbed CO_2 to 66 cm^3(STP)/g at 100 kPa. Lineshape analyses of wide-line ^{13}C NMR spectra measured at 195 K prove that the pillars undergo a fast rotational motion with jump rates around 2×10^3 s^{-1} at $p(CO_2) = 0$ (Figure 3a blue inset, 3c). The adsorption of the first lot of CO_2 ($p(CO_2) = 55$ kP) does not restrict the pillar dynamics significantly, which is
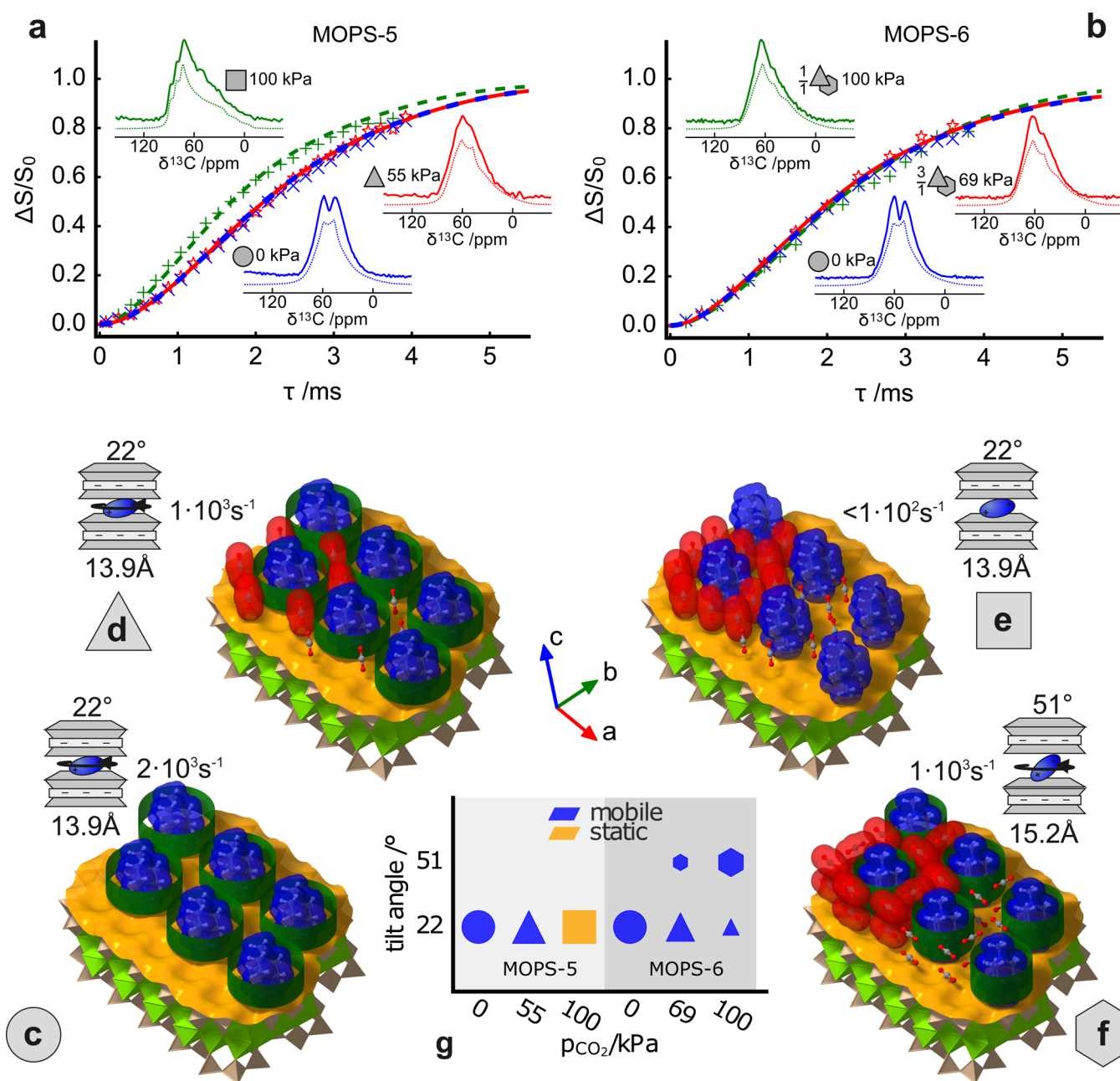
Figure 3. (a,b) Wideline 1D ^{13}C NMR spectra and distance measurements via $^{13}C\{^{19}F\}$ NMR CP-SEDOR dephasing curves at 195 K to assess both orientation and mobility of the pillars. (c−f) Volume plots of van der Waals surfaces of silicate layers (yellow), pillars (blue), and the borders of the dynamic volume occupied by the rotating pillar (green) to estimate the accessible pore volume and packing of CO_2 molecules (red) in the course of CO_2 adsorption. Panel g assigns these states to the measurements in panels a and b. The ratio of the phases is indicated in the insets in panels a and b in the case of more than one contributing structure. All NMR measurements were carried out with Me_2-$DABCO^{2+}$ ions carbon-13 enriched at both methyl groups in order to restrict the NMR simulations to the latter. The labeling of the axes refers to the conventional monoclinic unit cell although the clay basal surfaces display pseudohexagonal symmetry.

still faster than 1×10^3 s^{-1} (Figure 3a red inset, 3d). This suggests that CO_2 is adsorbed predominantly in permanent voids between rotating pillars. It might have appeared obvious for an intrinsically two-dimensional microporous material that the extra pore volume, which is filled for MOPS-5 beyond $p(CO_2) = 80$ kPa partial pressure, is generated by expanding the interlayer space against the Coulomb attraction. According to the classification suggested by Schneemann et al.,[21] this would be related to an interdigitated layer type of gate-opening. *In situ* powder X-ray diffraction (PXRD) measurements, however, show no significant increase of the initial d_{001}-value

of 13.9 Å (Figure 2d) over the complete pressure range. Consequently, the additional volume observed in CO_2 adsorption must have been created without expanding the interlayer space. As indicated by significantly broadened wideline ^{13}C NMR spectra at $p(CO_2) = 100$ kPa (Figure 3a green inset), the pillar rotation is frozen (jump rates $< 10^2$ s^{-1}) by CO_2 blocking, thereby reducing the effective dynamic radius of the pillar, making space for additional CO_2 molecules. According to the classification suggested by Schneemann et al.,[21] this result suggests that contrary to expectations, the mechanism resembles a linker rotation type of gate-opening.

Given the van der Waals length of a CO_2 molecule of 5.3 Å, one molecule each can be accommodated in a slightly inclined upright orientation in voids between three adjacent pillars in a pseudohexagonal packing (Figure 3d). With rotationally mobile pillars, the small gap between pillars adjacent along the pseudohexagonal a axes is, however, too narrow to accommodate CO_2 molecules. At gate-opening pressure, CO_2 molecules become then capable to squeeze into this gap while concomitantly blocking rotational motion (Figure 3e) and consequently doubling the adsorption capacity.

The gate-opening mechanism somewhat resembles phase transition related to configurational changes in linkers of MOFs[22] and of the zeolite imidazolate framework ZIF-7.[23] In these two cases, changes happen in the covalently linked framework whereas here the cooperative freezing is transmitted via nondirectional electrostatic interactions only.

The CO_2 adsorption of MOPS-5 is fully reversible and desorption involves, however, significant hysteresis. Contrary to MOPS behavior, gate-opening related to configurational changes in linkers of MOFs[22] and of the zeolite imidazolate framework ZIF-7[23] involved little to small hysteresis. This suggests a strong coupling of adsorption and structural changes due to the smaller additional pores generated by freezing pillar rotation (Figure 3e).

As to the nature of the restriction of the gate-opening phenomenon for CO_2 versus C_2H_2, we can only speculate. Structural (length, kinetic diameter: 3.3 Å for both) and physical properties (b.p.) are very similar, and MOPS-5 lacks specific functionality allowing for selective interactions. The two adsorbents, however, have quadrupole moments of opposite sign (-14.9×10^{-40} C m^2 and $+25.1 \times 10^{-40}$ C m^2).[10] The interaction of the basal oxygen atoms of the silicate layers with the hydrogen atoms of C_2H_2 versus the oxygen atoms of CO_2 molecules will therefore be quite different. The same applies to the lateral interaction with adjacent pillars. Because of the small differences between both adsorbates and the consequently quite similar host−guest interactions, we expect a high degree of correlation when separating both species from gas mixtures. The prediction of separation coefficients based on ideal absorbed solution theory would thus be meaningless and competition or break through experiments need to be carried out. In particular, parasitic uptake of C_2H_2 during the gate opening triggered by CO_2 might lead to significant deviations from ideal behavior. Because such experiments are quite demanding in time and amount of material needed, we refrain from presenting separation coefficients for the current work.

Pillar alignment and orientation in MOPS-5 were additionally probed as a function of CO_2 partial pressure at 195 K by determining carbon fluorine distances from the intercalated Me$_2$DABCO^{2+} cations (^{13}C enriched at the methyl groups) to the fluorine atoms in the silicate layers. To this end, solid-state NMR ^{13}C{^{19}F}SEDOR dephasing curves $\Delta S/S_0$ (Figure 3a) at three CO_2 partial pressures (0, 55, and 100 kPa) were analyzed.[24,25] The simulations employed extended ^{13}C^{19}F spin systems derived from an ordered pseudohexagonal arrangement of Me$_2$DABCO^{2+} cations in the interlayer space,[15,26] an interlayer distance of 13.9 Å (Figure 2d), and including the pillar dynamics derived from the ^{13}C wide-line NMR spectra. In all three cases, the simulations reproduce the trend for $\Delta S/S_0$ very well. The tilt angle of the Me$_2$-DABCO^{2+} ions with respect to the silicate layers is determined to be roughly 22° for all CO_2 partial pressures. However, although a fast pillar reorientation is

observed for $p(CO_2)$ = 0 and 55 kPa, the pillars are immobilized for p(CO_2) = 100 kPa (Figure 3g).

As mentioned in the introduction, the shape of the slit-type micropores may easily be fine-tuned by reducing the charge density of the silicate layers. This of course concomitantly reduces the Coulomb attraction of cationic interlayer space and anionic host layers. Surprisingly, we found that reducing the charge density alters the gate-opening mechanism to a conventional structural gate-opening involving an increase in volume.

The adsorption isotherm for CO_2 of low charge MOPS-6 resembles the one of MOPS-5 in the low pressure range where an initial uptake of 35 cm^3(STP)/g is observed at 20 kPa and a plateau is reached (Figure 2e). The gate-opening for MOPS-6 commences, however, at a much lower CO_2 pressure (>30 kPa) as compared to MOPS-5 (>80 kPa). Moreover, a discontinuity is observed in the adsorption isotherm with an inflection point at 69 kPa and a corresponding adsorption volume of 57 cm^3(STP)/g. The total adsorption capacity for MOPS-6 is considerably larger (76 cm^3(STP)/g) as compared to MOPS-5 (66 cm^3(STP)/g at 100 kPa) (Figure 2e). As with MOPS-5, the basal spacing of MOPS-6 does not change significantly upon adsorption to the first plateau (Figure 2f, B). At the inflection point (Figure 2f, C) two interlayer distances are observed at 13.9 and 14.6 Å. At 100 kPa (Figure 2f, D), three distinct interlayer distances are observed at 13.9, 14.6, and 15.2 Å (inset Figure 2f). In contrast to MOPS-5, partial expansion against the Coulomb attraction becomes feasible for the charge reduced MOPS-6 and the interlayer distance increases during CO_2 adsorption beyond gate-opening pressure. As for MOPS-5, for MOPS-6 gate-opening is restricted to CO_2 and no shift of the d_{001}-value was observed for the adsorption of C_2H_2 at 195 K (Figure S5).

The three PXRD peaks can be assigned to a nonexpanded (13.9 Å) and an expanded (15.2 Å) phase, as well as a regular interstratification of the two. The d_{001}-reflex (29.1 Å) of the latter is expected outside the accessible measurement range for the in situ PXRD and 14.6 Å corresponds to the d_{002}-value. In line with the higher total adsorption capacity of MOPS-6 as compared to MOPS-5, upon expansion of h_{int}, CO_2 needs to be adsorbed in a bilayer to fill completely the available pore space (Figure 3f). During the transition from point B to D in the adsorption isotherm, mixtures of expanded and nonexpanded interlayer structures at varying ratios are realized. As expected for an intrinsically two-dimensional pore system, adsorption in individual interlayers is not correlated and the total adsorption may be viewed as an overlay of the adsorption of the two types of interlayer arrangements. The ordered interstratification is, however, known to be a local thermodynamic minimum,[27,28] which explains the discontinuity in the isotherm at 69 kPa.

As for MOPS-5, pillar mobility, alignment and orientation were again probed by solid-state NMR techniques. Contrary to MOPS-5, for MOPS-6 line shape analyses of the wide-line ^{13}C NMR spectra (Figure 3b insets) reveal jump rates for the pillar rotation on the order of 1×10^3 s^{-1} for 0, 69, and 100 kPa CO_2 partial pressure indicating that contrary to MOPS-5, for MOPS-6 pillar rotation is not significantly hampered over the complete range of CO_2 pressures. Nevertheless, for 69 and 100 kPa the spectra consist of a superposition of two individual components, which we attribute to Me$_2$DABCO^{2+} ions in interlayer spaces of two different heights (Figure 2f). Moreover, the dephasing curves $\Delta S/S_0$ at $p(CO_2)$ = 0 kPa, $p(CO_2)$ = 69 kPa, and $p(CO_2)$ = 100 kPa all showed the same shape. This

indicates similar apparent distances between the methyl groups and the fluorine atoms in the silicate layers. Because at the same time PXRD showed that the interlayer distance partially increased by 1.1 Å at $p(CO_2) > 30$ kPa, this implies that the pillars in the expanded interlayers must have increased their tilt angle. Simulations of $\Delta S/S_0$ curves were achieved by superposition of varying ratios (Figure 3g) of nonexpanded and expanded interlayers (3:2 at 69 kPa and 2:3 at 100 kPa, respectively) and suggested a tilt angle of 50° for the latter (Figure 3f).

■ CONCLUSION

In summary, we found a new mechanism for gate-opening based on freezing pillar dynamics in MOPS. The mechanism is restricted to CO_2 and is not observed for C_2H_2. The mechanism underlying the additional CO_2 adsorption and the total adsorption capacity beyond gate-opening pressure can, moreover, be altered by tuning the charge density of the host layers (Figure 3g). With high charge density (MOPS-5), additional volume is created solely by freezing pillar rotation; whereas for low charge densities (MOPS-6), interlayers partially expand against the Coulomb attraction and concomitantly the tilt angle of elliptical pillars is increased.

Tuning the pillar density of MOPS allows for optimization of guest recognition without the need to explore different framework topologies, allowing for a straightforward rational design of microporous materials tailored for various industrially relevant gas mixtures in the future.

■ EXPERIMENTAL SECTION

Synthesis of MOPS-5 and MOPS-6. The stevensite $[Na_{0.47(3)}]^{inter}[Mg_{2.59(5)}Li_{0.17(3)}]^{oct}[Si_4]^{tet}O_{10}F_2$ used was synthesized via melt synthesis.[26,29] The high purity reagents (in total ~45 g) of SiO_2 (Merck, fine granular, calcined), MgF_2 (Chempur, 99.99%), MgO (Alfa Aesar 99.95%), Li_2SiO_3 (Alfa Aesar 99.95%), and Na_2O-$2SiO_2$-glass were weighed into a molybdenum crucible in an Ar atmosphere in accordance with a stoichiometric composition of $[Na_{0.6}]^{inter}[Mg_{2.6}Li_{0.2}\square]^{oct}[Si_4]^{tet}O_{10}F_2$ (target composition). Na_2O-$2SiO_2$-glass was produced by melting Na_2CO_3 (Aldrich, 99.9%) and SiO_2 (Merck, fine granular, calcined) in a 1:2 molar ratio at 1050 °C for 10 h to ensure complete release of carbon dioxide. The molybdenum crucible was sealed so as to be gastight using the procedure described elsewhere.[30] The crucible was heated in a graphite furnace (Graphit HT-1900, Linn High Therm) for the synthesis. To prevent inhomogeneity of the product owing to gravity segregation in the melt, the crucible was positioned horizontally in the furnace and rotated at 50 rpm. The crucible was heated from room temperature to 1750 °C (20 °C/min), left at 1750 °C for 1 h, then cooled to 1300 °C with a cooling rate of 50 °C/min, followed by a cooling rate of 10 °C/min from 1300 to 1050 °C, and finally it was quenched by switching off the power. The crucible was opened under an Ar atmosphere and the synthetic stevensite was stored in a Glovebox.

MOPS-5 was synthesized by pillaring stevensite (100 mg) hydrothermally four times for 12 h at 120 °C using 30 mg of $Me_2DABCOCl_2$ in 15 mL H_2O. For MOPS-6 the charge density was reduced prior to pillaring by first ion-exchanging the stevensite with Mg^{2+}. During annealing of Mg-stevensite at 250 °C for 12 h, part of the Mg^{2+} moves from the interlayer to the octahedral vacancies and thus the charge density of the silicate layers is reduced.[16]

Powder X-ray Diffraction and Physisorption. The powder X-ray diffraction (PXRD) patterns of the dry samples were recorded with a STOE Stadi P powder diffractometer (transmission geometry, $CuK_{\alpha1}$ radiation (λ = 1.540 56 Å), Ge monochromator, MYTHEN 1K detector) in a sealed capillary (Hilgenberg, diameter 0.5 mm). Prior to measurement, samples were dried for 24 h at 120 °C in high vacuum (10^{-6} mbar).

Argon adsorption measurements were performed using a Quantachrome Autosorb 1 at Ar(l) temperature (87.35 K) with Ar employing samples dried for 24 h at 100 °C in high vacuum. The pore sizes and volumes were calculated using a nonlocal DFT model (software version 2.11, Ar on zeolite/silica, cylindrical pores, equilibrium model). The volume-weighted median micropore width corresponds to the point where the total pore volume in the micropore regime (<2 nm) was half filled.

The adsorption isotherms for C_2H_2 (KOATSU GAS KYOGYO CO. LTD, ≥99.9999 vol %) and CO_2 (TAIYO NIPPON SANSO, ≥99.995 vol %) were performed using an automatic volumetric adsorption apparatus (BELSORP-18PLUS or BELSORP-max, Bel-Japan, Inc.) connected to a cryostat system. The samples were dried under high vacuum (below 10^{-2}Pa) at 100 °C for 12 h.

The coincident PXRD/adsorption measurements were carried out using a Rigaku UltimaIV with Cu $K\alpha$ radiation connected to a BELSORP-18PLUS volumetric adsorption apparatus (Bel Japan, Inc.). Those apparatuses were synchronized with each other and PXRD patterns were obtained at each equilibrium point of the sorption isotherms.

Solid-State NMR. To restrict the analysis to the methyl groups, all NMR measurements were carried out with Me_2-$DABCO^{2+}$ ions that were carbon-13 enriched at both methyl groups. All wide-line ^{13}C-cross-polarization (CP) and $^{13}C\{^{19}F,^1H\}$ cross-polarization spin echo double resonance (CP-SEDOR) experiments[24,25] were carried out on an Avance II 300 FT NMR spectrometer (Bruker) with resonance frequencies of 300.13, 75.47, and 282.40 MHz for ^1H, ^{13}C, and ^{19}F, respectively. Saturation combs were applied prior to the experiments and during the acquisition period proton broadband decoupling with a continuous wave sequence and a nutation frequency of 83.33 kHz was applied. The CP experiments were performed using squared ^1H lock pulses with lengths (τ_{CP}) of 5.0 and 3.0 ms, nutation frequencies for ^{13}C and ^1H of 60.5 kHz and a recycle delay of 1.5 s. All $^{13}C\{^{19}F\}$ CP-SEDOR measurements were performed at 195 K. The nutation frequencies of the 180° pulses during the CP-SEDOR pulse train were adjusted to 50 and 65 kHz for ^{19}F and ^{13}C, respectively. For the CP block, similar conditions as for the individual CP measurements were used. Each experimental data point was recorded at a dephasing time, τ, which was incremented in 80 μs steps. 800 and 1024 repetitions were accumulated for each FID for the unloaded and the fully loaded sample, respectively. A total of 104 rows/FIDs were recorded with alternating between a dephasing and a reference experiments after each step. The sample was packed in a home-built 3.0 mm inner diameter PEEK sample holder in a closed loop with either a fully loaded CO_2 or with He for unloaded CO_2 to prevent the moisture adsorption. The sample was heated to 150 °C for 12 h in the NMR probe under vacuum to remove adsorbed water molecules. The CP-SEDOR data were plotted as $\Delta S/S_0 = (S_0-S)/S_0$ against the dephasing time τ with S_0 and S being the spectral intensity of the reference and dephased data set for each τ. Simulations of the CP-SEDOR curves were carried out using the program package SIMPSON[31] and an in-house Python library based on analytic solutions. The library also implements the simulation of one-dimensional (1D) spectra under the influence of jump motion[32] and SEDOR curves based on refs 33, 34. The spin systems up to eight spins have been created with the Python library using the crystal structure of Na-Stevensite and a geometry-optimized structure of Me_2DABCO^{2+}. Simulations include the carbon−fluorine dipolar couplings and take into account fluorine homonuclear couplings as well as a correction for residual molecular motion and spin-system size cutoff effects.

Hyperpolarized ^{129}Xe NMR. All hyperpolarized ^{129}Xe NMR experiments were acquired using a home-built polarizer. A gas mixture composed of 1% (Xe):3% (N_2):96% (He) (by volume) was used to polarize ^{129}Xe using 80 W of diode laser power tuned to the Rb D_1 line ($\lambda \cong$ 794 nm), providing about 5% total polarization. The total overpressure of 4 bar was maintained throughout static as well as MAS experiments.

The static 1D variable temperature HP ^{129}Xe NMR spectra were recorded on a Bruker Avance II-300 spectrometer operating at a frequency of 83.47 MHz. A commercial wide-line double resonance

probe (Bruker) was used. HP ^{129}Xe was incorporated through a home-built 3.0 mm inner diameter PEEK sample holder. The HP Xe-gas chemical shift (0 ppm) was used as an internal standard reference for all experiments. One-dimensional ^{129}Xe static NMR spectra were acquired with a 90° pulse length of 4.5 μs, and a recycle delay of 1.0 s. The flow rates of the Xe/N$_2$/He gas mixture in the circulating loop were adjusted to around 700 sccm for all static measurements.

One-dimensional ^{129}Xe MAS NMR spectra were performed using a commercial 7 mm MASCAT probe (Bruker) utilizing a stream of CF-HP ^{129}Xe gas mixture. However, the gas mixture is vented to the atmosphere instead of circulating in a closed loop. The gas flow is created by a pressure difference between the pumping cell ($p \sim 4.0$ bar) and atmosphere, i.e., at the rotor. The ^{129}Xe MAS NMR spectra were acquired with a single pulse sequence, a 90° pulse length of 4.5 μs, and a recycle delay of 1.0 s.

■ ASSOCIATED CONTENT

Ⓢ Supporting Information

The Supporting Information is available free of charge on the ACS Publications website at DOI: 10.1021/jacs.6b11124.

Figure S1−S5, showing Ar physisorption isotherms and pore size distributions for MOPS-5 and 6; MAS and wide-line ^{129}Xe-NMR spectra; X-ray diffraction patterns for MOPS-5 and 6; and C$_2$H$_2$ adsorption isotherm of MOPS-6 (PDF)

■ AUTHOR INFORMATION

Corresponding Authors
*juergen.senker@uni-bayreuth.de
*ryotaro.matsuda@apchem.nagoya-u.ac.jp
*kitagawa@icems.kyoto-u.ac.jp
*josef.breu@uni-bayreuth.de

ORCID Ⓘ
Josef Breu: 0000-0002-2547-3950

Author Contributions
M.M.H. and J.B. designed synthesis and characterization of the materials. M.M.H., M.R., K.B., J. S., H.S., S.K., R.M., and J.B. contributed to the paper. H.S., L.L., M.M.H., and R.M. performed the in situ combined physisorption and PXRD experiments. Y.S.A., T.W.K., K.B., and J.S. designed and performed the solid-state NMR experiments and the corresponding analysis.

Notes
The authors declare no competing financial interest.

■ ACKNOWLEDGMENTS

■ REFERENCES

(1) Slater, A. G.; Cooper, A. I. *Science* **2015**, *348*, aaa8075.
(2) Schoedel, A.; Ji, Z.; Yaghi, O. M. *Nat. Energy* **2016**, *1*, 16034.
(3) Li, J. R.; Kuppler, R. J.; Zhou, H. C. *Chem. Soc. Rev.* **2009**, *38*, 1477.
(4) Zhang, X. Y.; Liu, D. X.; Xu, D. D.; Asahina, S.; Cychosz, K. A.; Agrawal, K. V.; Al Wahedi, Y.; Bhan, A.; Al Hashimi, S.; Terasaki, O.; Thommes, M.; Tsapatsis, M. *Science* **2012**, *336*, 1684.
(5) Liu, Y.; Pan, J. H.; Wang, N. Y.; Steinbach, F.; Liu, X. L.; Caro, J. *Angew. Chem., Int. Ed.* **2015**, *54*, 3028.
(6) Cui, X.; Chen, K.; Xing, H.; Yang, Q.; Krishna, R.; Bao, Z.; Wu, H.; Zhou, W.; Dong, X.; Han, Y.; Li, B.; Ren, Q.; Zaworotko, M. J.; Chen, B. *Science* **2016**, *353*, 141.
(7) Bloch, E. D.; Queen, W. L.; Krishna, R.; Zadrozny, J. M.; Brown, C. M.; Long, J. R. *Science* **2012**, *335*, 1606.
(8) Zhang, Z. J.; Xiang, S. C.; Chen, B. L. *CrystEngComm* **2011**, *13*, 5983.
(9) Matsuda, R.; Kitaura, R.; Kitagawa, S.; Kubota, Y.; Belosludov, R. V.; Kobayashi, T. C.; Sakamoto, H.; Chiba, T.; Takata, M.; Kawazoe, Y.; Mita, Y. *Nature* **2005**, *436*, 238.
(10) Eguchi, R.; Uchida, S.; Mizuno, N. *Angew. Chem., Int. Ed.* **2012**, *51*, 1635.
(11) Krause, S.; Bon, V.; Senkovska, I.; Stoeck, U.; Wallacher, D.; Többens, D. M.; Zander, S.; Pillai, R. S.; Maurin, G.; Coudert, F.-X.; Kaskel, S. *Nature* **2016**, *532*, 348.
(12) Sato, H.; Kosaka, W.; Matsuda, R.; Hori, A.; Hijikata, Y.; Belosludov, R. V.; Sakaki, S.; Takata, M.; Kitagawa, S. *Science* **2014**, *343*, 167.
(13) Alhamami, M.; Doan, H.; Cheng, C. H. *Materials* **2014**, *7*, 3198.
(14) Herling, M. M.; Breu, J. *Z. Anorg. Allg. Chem.* **2014**, *640*, 547.
(15) Baumgartner, A.; Sattler, K.; Thun, J.; Breu, J. *Angew. Chem., Int. Ed.* **2008**, *47*, 1640.
(16) Herling, M. M.; Kalo, H.; Seibt, S.; Schobert, R.; Breu, J. *Langmuir* **2012**, *28*, 14713.
(17) Stöter, M.; Kunz, D. A.; Schmidt, M.; Hirsemann, D.; Kalo, H.; Putz, B.; Senker, J.; Breu, J. *Langmuir* **2013**, *29*, 1280.
(18) Mermut, A. R.; Lagaly, G. *Clays Clay Miner.* **2001**, *49*, 393.
(19) Demarquay, J.; Fraissard, J. *Chem. Phys. Lett.* **1987**, *136*, 314.
(20) Keenan, C. D.; Herling, M. M.; Siegel, R.; Petzold, N.; Bowers, C. R.; Rössler, E. A.; Breu, J.; Senker, J. *Langmuir* **2013**, *29*, 643.
(21) Schneemann, A.; Bon, V.; Schwedler, I.; Senkovska, I.; Kaskel, S.; Fischer, R. A. *Chem. Soc. Rev.* **2014**, *43*, 6062.
(22) Yang, W.; Davies, A. J.; Lin, X.; Suyetin, M.; Matsuda, R.; Blake, A. J.; Wilson, C.; Lewis, W.; Parker, J. E.; Tang, C. C.; George, M. W.; Hubberstey, P.; Kitagawa, S.; Sakamoto, H.; Bichoutskaia, E.; Champness, N. R.; Yang, S.; Schröder, M. *Chem. Sci.* **2012**, *3*, 2993.
(23) Gücüyener, C.; van den Bergh, J.; Gascon, J.; Kapteijn, F. J. *J. Am. Chem. Soc.* **2010**, *132*, 17704.
(24) Emshwiller, M.; Hahn, E. L.; Kaplan, D. *Phys. Rev.* **1960**, *118*, 414.
(25) Kaplan, D. E.; Hahn, E. L. J. *J. Phys. Radium* **1958**, *19*, 821.
(26) Stöcker, M.; Seidl, W.; Seyfarth, L.; Senker, J.; Breu, J. *Chem. Commun.* **2008**, 629.
(27) Stöter, M.; Biersack, B.; Rosenfeldt, S.; Leitl, M. J.; Kalo, H.; Schobert, R.; Yersin, H.; Ozin, G. A.; Förster, S.; Breu, J. *Angew. Chem., Int. Ed.* **2015**, *54*, 4963.
(28) Stöter, M.; Biersack, B.; Reimer, N.; Herling, M.; Stock, N.; Schobert, R.; Breu, J. *Chem. Mater.* **2014**, *26*, 5412.
(29) Kalo, H.; Möller, M. W.; Kunz, D. A.; Breu, J. *Nanoscale* **2012**, *4*, 5633.
(30) Breu, J.; Seidl, W.; Stoll, A. J.; Lange, K. G.; Probst, T. U. *Chem. Mater.* **2001**, *13*, 4213.
(31) Bak, M.; Rasmussen, J. T.; Nielsen, N. C. J. *J. Magn. Reson.* **2000**, *147*, 296.
(32) Vold, R. L.; Hoatson, G. L. J. *J. Magn. Reson.* **2009**, *198*, 57.
(33) Goetz, J. M.; Schaefer, J. J. *J. Magn. Reson.* **1997**, *127*, 147.
(34) Mueller, K. T. J. *J. Magn. Reson., Ser. A* **1995**, *113*, 81.